scientific reports

Check for updates

OPEN

# Unravelling the dynamics of the maturation protein in MS2 bacteriophage via molecular simulations

Srdan Masirevic[1,7], Jan K. Marzinek[1,7], Jiquan Liu[2], C. Mark Maupin[3], Stephen J. Fox[4], Chandra S. Verma[1,5,6]✉ & Peter J. Bond[1,6]✉

**The MS2 bacteriophage capsid serves as a model system for studying viral structure and function. Mature MS2 virus consists of 178 capsid proteins and a single maturation protein (MP), which is essential for host receptor binding and infection initiation. Despite its critical role, the dynamic behavior of the capsid with the MP remains poorly understood. To address this, we conducted 0.5 µs all-atom molecular dynamics (MD) simulations of the MS2 capsid with and without the MP, revealing key insights into its structural dynamics. Our simulations showed that MP exhibits high flexibility, particularly in the "tip" and "side-loop" regions, which undergo significant motions that likely enhance its ability to engage with the F-pilus receptor. Detailed analysis of MP conformational states revealed that loop rearrangements around H357 enable transient switching between "semi-closed" and "open" conformations, suggesting a conformational selection mechanism for pilus binding. Additionally, ion interaction analyses revealed distinct sodium and chloride binding patterns, where sodium ions were mostly found at the outer capsid shell, while chloride ions interacted with the basic residues on the RNA-facing side. We also found that the presence of the MP enhances salt-bridge interactions, contributing to increased capsid stability, yet it does not significantly alter the pore sizes of pentameric and hexameric units. Together, these findings provide new insights into the functional role of the MP, highlighting its contribution to capsid stability and host receptor engagement. This study offers a foundation for understanding capsid dynamics relevant to viral infectivity and may guide future rational strategies aimed at disrupting host-virus interactions.**

**Keywords** MS2 bacteriophage, Maturation protein, Molecular dynamics simulations, Viral infectivity, Protein dynamics, Capsid stability, Ion interactions

**Abbreviations**

| | |
|---|---|
| MD | Molecular dynamics |
| CP | Capsid protein |
| MP | Maturation protein |

MS2 bacteriophage is a small, icosahedral, non-enveloped, single-stranded RNA (+ssRNA) virus that infects Gram-negative bacteria, particularly *Escherichia coli*. Its capsid measures approximately 23–28 nm in diameter and contains a single copy of the maturation protein (MP), along with 178 copies of the capsid protein (CP). Each CP is composed of 129 amino acid residues, forming a five-stranded β-sheet that faces the capsid interior and a hairpin structure with two helices on the outside[1]. The primary building block of MS2 is the CP dimer, which exists in two forms: symmetric (C/C) dimers located at the 2-fold axes and asymmetric (A/B) dimers positioned at the 5-fold and 3-fold axes[2]. In the symmetric (C/C) dimer arrangement, both CP subunits adopt

[1]Bioinformatics Institute (BII), Agency for Science, Technology and Research (A*STAR), 30 Biopolis Street, #07-01 Matrix, Singapore 138671, Republic of Singapore. [2]Procter and Gamble, The Metropolis 11 North Buona Vista Drive, Singapore 138589, Republic of Singapore. [3]Pacific Northwest National Laboratory, Richland, WA 99352, USA. [4]Procter and Gamble, Reading RG2 0RX, UK. [5]School of Biological Sciences, Nanyang Technological University, 50 Nanyang Drive, Singapore 637551, Republic of Singapore. [6]Department of Biological Sciences, National University of Singapore, 16 Science Drive 4, Singapore 117558, Republic of Singapore. [7]Srdan Masirevic and Jan K. Marzinek contributed equally to this work. ✉email: chandra@bii.a-star.edu.sg; peterjb@bii.a-star.edu.sg

the same conformation, whereas in the asymmetric (A/B) dimer form, the two CP subunits adopt different conformations. This difference allows dimers to accommodate the geometric constraints of the icosahedral capsid, facilitating proper assembly at different symmetry axes.

The MP replaces one of the 90 CP dimers, spanning the entire thickness of the viral shell and introducing a point of asymmetry to the viral capsid. This structural asymmetry is closely linked to the MP's known functional roles in host receptor binding and genome packing[3]. Previous studies have emphasized that this asymmetry plays a crucial role in shaping the structural dynamics and functional mechanisms of the virus[4,5]. In wild-type (wt) MS2 virions, a single MP is present and is essential for binding to the host's F-pili, a critical step in bacterial infection. The absence of the MP or mutations in its sequence render MS2 virions non-infectious, as they lose the ability to bind to pili, highlighting its indispensable role in the infection process[6].

The MS2 bacteriophage is a widely studied model for understanding virus structure and function, with its architecture extensively characterized through X-ray crystallography and cryo-electron microscopy (cryo-EM). While early structural studies revealed the capsid's quasi-icosahedral symmetry, the MP – a key player in infection – remained unresolved. More recent cryo-EM work successfully resolved the MP structure, including in complex with the bacterial F-pili, highlighting its role in host receptor binding and orientation during infection[3].

Structurally, the MP comprises an α-helical core and an extended β-sheet domain[7]. Two functionally relevant regions have previously been highlighted: (i) the "tip" at the end of the β-sheet, which forms electrostatic and hydrophobic interactions with the F-pilus (notably involving residues like R36 and R99); and (ii) a flexible "side-loop" adjacent to H357, implicated in conformational transitions that may facilitate pilus engagement and infectivity. These motifs are conserved in MS2 and appear structurally and functionally distinct from those in related ssRNA bacteriophages such as Qβ, whose maturation protein exhibits a different fold and host interaction strategy[8].

Despite this structural knowledge, the dynamics of the MP—and its influence on the capsid and infection process—remain underexplored. Previous MD simulations of MS2, including work by Farafonov and Nerukh[4] and more recent all-atom simulations with encapsulated RNA[9], have contributed valuable insights into capsid mechanics and stability.

Here, we performed 0.5 μs all-atom MD simulations of the complete MS2 capsid with and without the MP and investigate MP dynamics and its functional coupling with surrounding CPs. Our analysis reveals marked differences in salt-bridge distributions, ion interactions, and structural flexibility between the two systems. Notably, the CPs surrounding the MP exhibit a higher density of salt bridges, suggesting a stabilizing effect of the MP on adjacent CPs. Furthermore, principal component analysis (PCA) and conformational clustering analysis indicate that key interacting motifs in the MP (tip and side-loop) undergo dynamic motions that may prime the MP for binding the F-pilus. These findings deepen our understanding of MP function and highlight potential structural targets for antiviral strategies aimed at disrupting host-virus interactions.

## Results & discussion

### Structural stability

MD simulations of both MS2 with and without MP exhibited stable virion conformations over the entire 0.5 μs trajectories, as indicated by the RMSD of protein backbone atoms for the entire capsid shell (Figure S1). To evaluate the structural convergence and stability of the capsid systems, we assessed convergence of both trajectories and examined various global metrics over 100 ns blocks, including radius of gyration, total number of hydrogen bonds, ion–protein contacts, and pore diameter. These observables are commonly used to assess compactness, hydration, electrostatics, and potential expansion/contraction of viral capsids. For all metrics, the final 200 ns showed stable values with progressively decreasing standard deviations, suggesting convergence had been achieved (Figure S2, Tables S1 and S2). Both systems maintained their structure close to the experimental structure, with the $MS2_{MP}$ system exhibiting slightly more structural drift, with the RMSD plateauing at ~ 0.4 nm, in comparison to the $MS2_{No-MP}$ system where the RMSD plateaued at ~ 0.38 nm. The diameter of the capsid remained near the experimental value for both systems, swelling slightly from ~ 24.3 nm to ~ 25.0 nm by the end of each simulation, presumably because of the relaxation of the protein shell in the absence of RNA. Simulated per-residue atomic B-factors revealed elevated flexibility in the loop regions of both hexameric and pentameric loops comprising pore regions of the CPs, regardless of the presence of the MP. Within the MP itself, increased flexibility was observed in the β-sheet domain (tip) and the side-loop region (red), whereas the α-helical core remained relatively rigid (blue) (Fig. 1a). The B-factor difference (ΔB-factor) map (Fig. 1b) highlights that this increase in flexibility is not confined to CPs immediately adjacent to the MP but is distributed across multiple loop regions throughout the capsid. This suggests that presence of the MP introduces asymmetry that propagates dynamic perturbations, especially affecting structurally less constrained loop regions. A few regions, such as CP β-strands and helices, exhibit increased rigidity, possibly reflecting compensatory stabilization in response to the altered shell dynamics.

### Ion uptake

Analysis of ion uptake revealed distinct patterns of sodium and chloride distribution across the MS2 capsid inner and outer surfaces. In both $MS2_{MP}$ and $MS2_{No-MP}$ systems, sodium ions were predominantly found on the outer shell of the capsid, with the highest density located at the interfaces between three capsid dimers (Fig. 2a, b). This trimeric interface was particularly enriched with sodium ions, as evidenced by the per-residue occupancy, which highlighted the Y129 carboxylate C-termini, S2 side chain hydroxyls, and F4 backbone oxygens as the key binding sites for sodium ions (Fig. 2c). In contrast, chloride ions were concentrated on the inner (RNA-facing) side of the capsid, interacting with the basic residues of both the capsid proteins (Fig. 2d). Per-residue chloride occupancy showed strong interactions with basic residues in both the capsid dimers (Fig. 2e-g) and the MP (Fig. 2i), with additional involvement of basic residues in the MP-RNA complex (Fig. 2h). These ion interactions

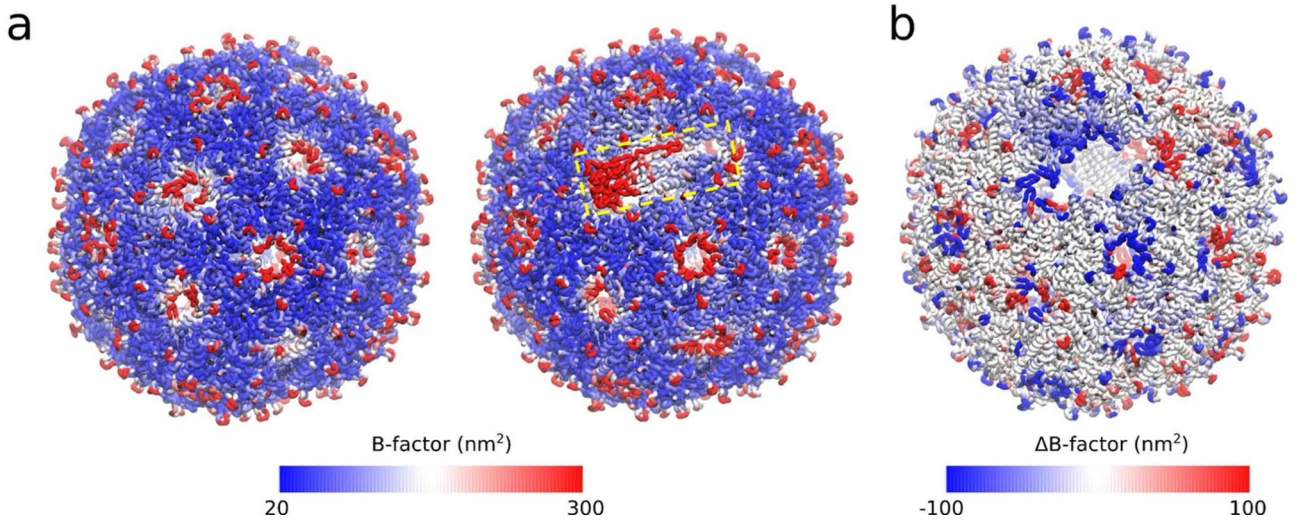



**Fig. 1**. Per-residue atomic displacement parameter (B-factor) of the MS2 capsid. (**a**) B-factor averaged over the 0.5 μs trajectory for the $MS2_{No-MP}$ (left) and $MS2_{MP}$ (right) systems. The location of MP is shown with a yellow dotted rectangular box. (**b**) B-factor difference (ΔB-factor) was calculated by subtracting the B-factors of the $MS2_{No-MP}$ system from those of the $MS2_{MP}$ system with positive values (red) indicating higher atomic displacement in the $MS2_{MP}$ system. The protein is shown in cartoon representation, colored from red (positive ΔB-factor) through white to blue (negative ΔB-factor), with values indicated in the legend.

likely play a crucial role in maintaining local structural stability in the RNA-depleted regions of the capsid, by mimicking the electrostatic interactions normally provided by RNA phosphates.

## Principal component analysis of MS2 capsid shell dynamics

Principal component analysis (PCA) revealed significant collective motions within the $MS2_{MP}$ system, with the first principal component (PCA1) indicating notable dynamics primarily in the MP and its associated loops (Fig. 3a). When PCA was independently applied to the MP and its ten surrounding dimers, pronounced movements were observed specifically in these regions (Fig. 3b, c). The porcupine plot illustrates the extreme states of PCA1, highlighting substantial conformational changes in both the MP and its neighboring loops (Fig. 3d). These results suggest that the external (non-RNA bound) surface of the MP and its associated loop regions undergo pronounced "outward motions", which may play a crucial role in the functional dynamics of the MS2 capsid. One possibility is that these flexible motions facilitate initial contact with the host's F-pilus receptor — consistent with cryo-EM observations (PDB ID: 6NM5) showing that the tip and β-sheet face of the MP directly interact with several F-pilin subunits. Notably, this interaction involves a flexible surface defined by residues R36, R99, F92, and F94, which are located in highly dynamic regions. An alternative — but not mutually exclusive — hypothesis is that these "outward motions" represent a preparatory conformational state that weakens MP–capsid contacts, thus priming the MP for detachment. This detachment may be a prerequisite for RNA release through local capsid destabilization. As proposed by Meng et al.[3], binding of MS2 to the F-pilus does not immediately trigger genome release, suggesting that additional conformational changes in the MP or capsid are required. Our data support a model where MP flexibility — especially in the side loop region, and the tip — could serve as a molecular switch for disengaging MP from the capsid, possibly induced or amplified by host-cell binding forces. This dynamic priming mechanism may help bridge structural observations with the still poorly understood mechanism of genome ejection in ssRNA phages.

## Pore dynamics

The MS2 capsid contains 32 pores (12 pentameric and 20 hexameric pores), one at the center of each icosahedral pentameric and hexameric unit, contributing to the overall architecture and facilitating molecule exchange. To investigate the influence of the MP on these structural features, the distribution of pentameric and hexameric pore radii was analysed over the simulation time for both the $MS2_{MP}$ and $MS2_{No-MP}$ systems. Across all pores, both systems displayed similar radii distributions, with the most common pore size being approximately 2 nm (Figure S3). However, statistical analysis revealed significant differences in the mean pore radii between the $MS2_{MP}$ and $MS2_{No-MP}$ systems for both pentameric and hexameric pores ($p.<0.05$). For pentameric pores, the mean radius of $MS2_{MP}$ (2.010 nm) was slightly smaller than that of $MS2_{No-MP}$ (2.070 nm). On the other hand, for hexameric pores, the mean radius of $MS2_{MP}$ (2.151 nm) was slightly larger than that of $MS2_{No-MP}$ (2.096 nm). Although the statistical analysis revealed significant differences in the mean pore radii, the observed differences in the mean radii are minor. Given the dynamic nature of the system, we believe that these small differences are unlikely to have substantial biological or functional significance.

To confirm that our simulations yield physically realistic pore dimensions, we compared the MD-derived pore radii to two static references: the final simulation frame and the cryo-EM structure of MS2 with RNA (PDB: 5MSF) from Rowsell et al.[19]. In both pentameric and hexameric pores, the final frame values closely matched

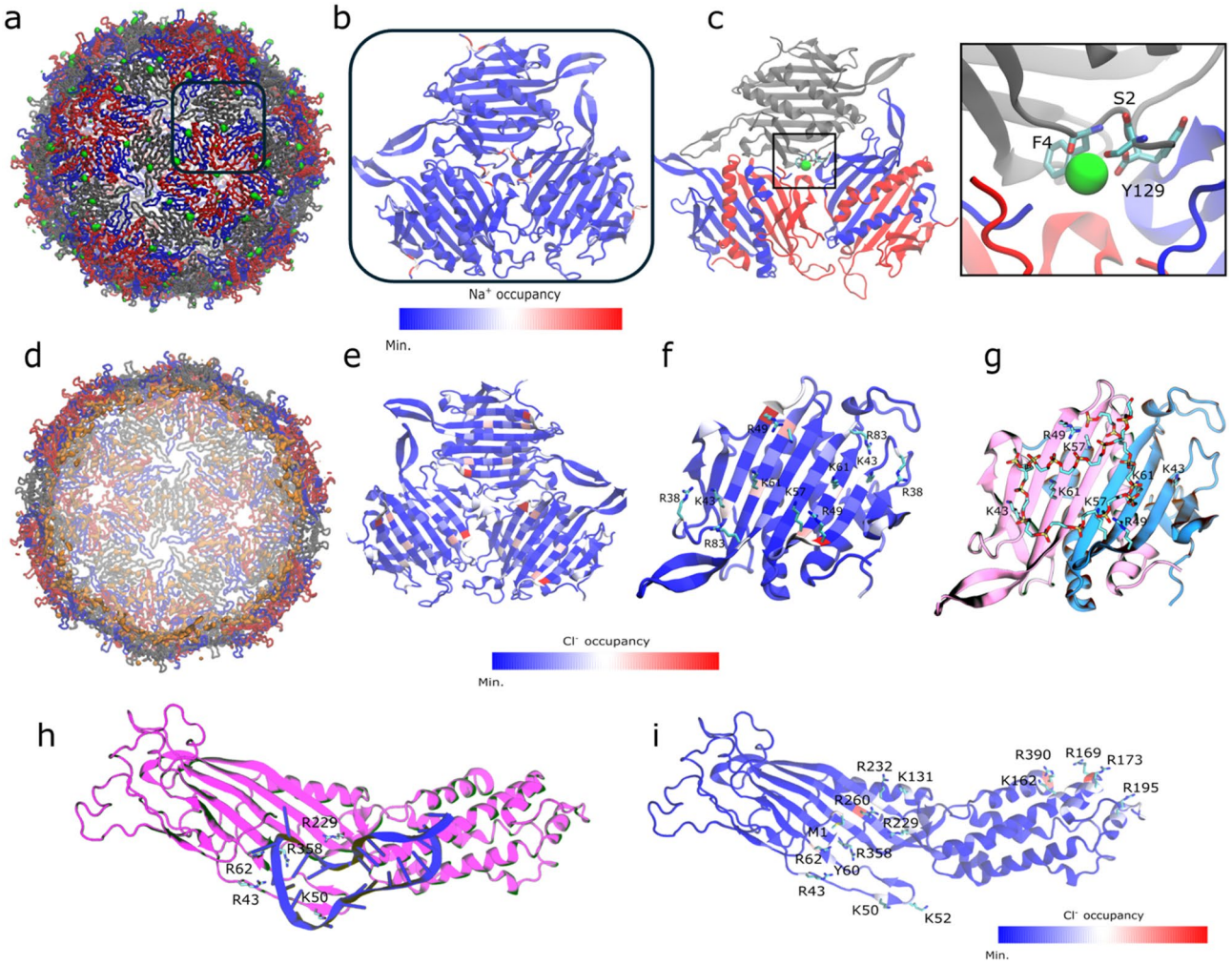



**Fig. 2**. Analysis of sodium ($Na^+$) and chloride ($Cl^-$) ion interactions with the MS2 capsid. **(a)** Density of sodium across the entire capsid in the MS2_MP system. **(b)** Sodium occupancy in a CP trimer of dimers. **(c)** CP trimer of dimers interface with sodium binding sites (Y129, S2, F4). **(d)** Density of chloride ions on the capsid interior surface. **(e)** Chloride occupancy in CP trimeric dimers. **(f)** CP dimer unit showing basic residue side chains that interact with chlorides. Experimental structures are shown of: **(g)** RNA – dimer capsid complex highlighting all protein basic residues involved in this interaction; and **(h)** MP – RNA complex with depicted protein basic residue side chains involved in this interaction. **(i)** Per-residue chloride occupancy fraction is shown for MP with interacting basic residues highlighted. Protein is shown in cartoon representation in all panels. RNA is shown in licorice representation in **(g)** and cartoon representation in **(h)**. In **(a)**, **(c)** and **(d)** CP is coloured according to asymmetric (blue/red) and symmetric dimers (grey/grey)

the mean values observed in the 400–500 ns interval, indicating convergence. The 5MSF structure also exhibited comparable pore sizes, especially for the hexameric pores. A detailed comparison is provided in Tables S3 and S4.

## Salt bridges

To evaluate the role of salt bridges in capsid stability, we analysed the frequency distribution of salt bridge contacts exclusively between CPs in both the $MS2_{MP}$ and $MS2_{No-MP}$ systems, eliminating potential bias from salt bridges involving the MP. The results showed that the $MS2_{MP}$ system exhibited a higher number of CP-CP salt bridges compared to the $MS2_{No-MP}$ system, indicating that the presence of the MP indirectly enhances the stability of the capsid by promoting increased CP-CP interactions (Figure S4). Salt bridges play a critical role in maintaining the structural integrity of icosahedral viral capsids, contributing to protein-protein interaction networks that stabilize the assembly. By focusing on CP-CP interactions, our analysis demonstrates that the MP's presence enhances inter-subunit connectivity, reinforcing the capsid structure against destabilizing forces. These findings highlight the MP's broader influence on the stability of the MS2 capsid, beyond its direct interactions with CPs or its role in receptor binding.

To further dissect this effect, we stratified the CPs in the $MS2_{MP}$ system into two groups: the 10 CPs dimers (20 CPs) directly adjacent to the MP, and the remaining 159 CPs. Histograms of salt bridge distributions were

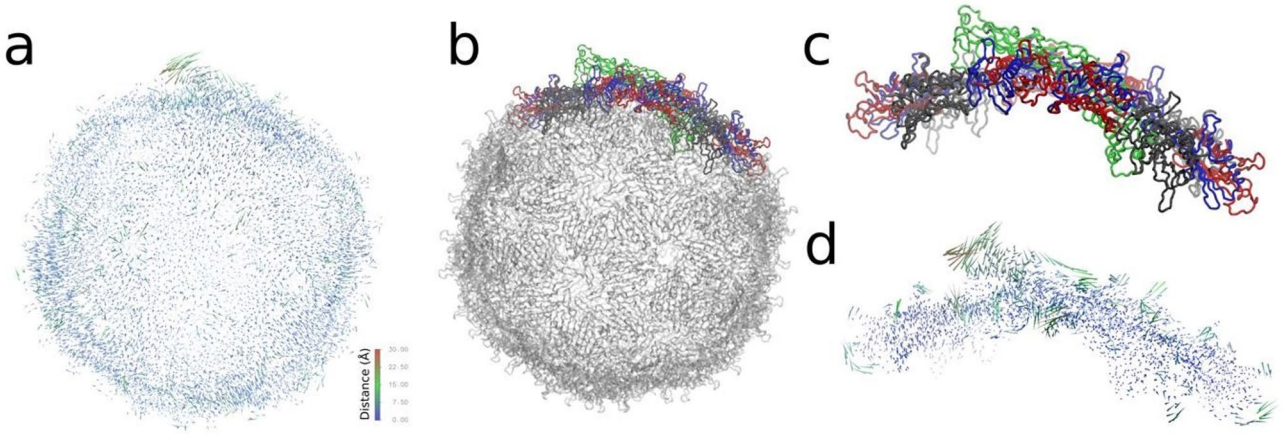



**Fig. 3**. PCA of $MS2_{MP}$ system. **(a)** Porcupine plot showing extreme states of PCA1 of the entire capsid. **(b)** PCA was independently conducted on MP together with ten surrounding dimers, as shown **(c)** "zoomed in" on this complex. **(d)** Porcupine plot showing extreme states of PCA1 of the MP with surrounding CP dimers. In panels **(b)** and **(c)** protein is shown in cartoon representation: MP (green), ten surrounding dimers are colored as asymmetric (blue/red), and symmetric dimers (grey/grey). In **(b)** the remainder of the capsid is shown as transparent grey

normalized with respect to the number of CPs analysed. Our data revealed no clear distinction: CPs adjacent to the MP formed a similar number of salt bridges per CP as both the remaining CPs in the same system as well as all CPs in the $MS2_{No\text{-}MP}$ system (Figure S5).

### Maturation protein dynamics

The dynamic properties of the MP were analysed by calculating the RMSD of the protein backbone atoms as well as the tilt angle of MP with respect to the capsid shell surface over the 0.5 μs simulation. The RMSD of the MP was significantly higher than the average RMSD for the 178 CPs in the $MS2_{MP}$ system, indicating that its dynamics are less constrained as a result of a lack of surrounding symmetric protein units (Figure S6, top). The tilt angle of the MP with respect to the shell surface showed substantial fluctuations, varying between ~ 20–90 degrees compared to its experimentally determined tilt of 20 degrees, observed in the receptor-bound state. This result is expected, as the experimental structure was determined in complex with the F-pilus receptor; however, it confirms that the MP is a highly dynamic unit in the absence of the receptor, suggesting its flexibility may play a crucial role in the infection process, potentially helping to "scan" the bacterial surface for the pilus receptor (Figure S6, bottom). 2D RMSD matrix analysis of the MP revealed distinct conformational states, indicated by clusters of RMSD values along the diagonal (Figure S7). Additionally, PCA performed specifically on the MP (as opposed to the entire capsid) revealed that the largest collective motions occurred in the 'tip' and 'side-loop' regions, while the rest of the MP remained relatively stable. Our MD simulations highlight substantial dynamics in the loop region surrounding H357 of the MP (Fig. 4).

In the experimental MS2/F-pilus complex structure (PDB ID: 6NM5), H357, R36, and R39 form a network of electrostatic interactions with D7 and D23 on the F-pilus, stabilizing the interface. Additional hydrophobic contacts from the MP 'tip' further anchor the interaction. To investigate whether our simulations capture these interactions, we extracted representative MP conformations and aligned them with the experimental structure (Figures S8 and S9). This revealed that the MP samples both "open" and "semi-closed" loop states, with the tip region adopting geometries that enable residues R36, R99, and H357 to occupy their known binding positions. These results support a conformational selection model, whereby flexible side-loop and MP tip dynamics allow the MP to transiently explore binding-competent states prior to engaging the F-pilus. Analysis of the MP tilt angle, RMSD, and local H357-protein interactions revealed that the opening of the loop surrounding H357 may help to align the MP in a conformation suitable for effective binding (Fig. 4). The contact analysis further highlighted the dynamic interactions between H357 and the adjacent side-loop (residues L40–P50), suggesting that these movements are likely critical for the MP's role in viral infectivity (Figure S10).

## Conclusions and future directions

Our all-atom MD simulations provide critical insights into the dynamic behaviour of the MS2 bacteriophage and the role of the MP in its infectivity. RMSD and PCA analyses reveal that the MP is highly flexible, particularly in the 'tip' and 'side-loop' regions, including the loop surrounding H357. These flexible motifs likely facilitate interactions with the host's F-pilus, by enhancing accessibility for receptor binding. Rather than indicating a lack of structural change, our findings highlight the importance of localized conformational mobility in enabling the MP's functional interactions.

While the MP's flexibility and interactions with neighboring dimers contribute to its functional role, the overall capsid structure remains stable, with no functionally significant changes observed in the pore radii of

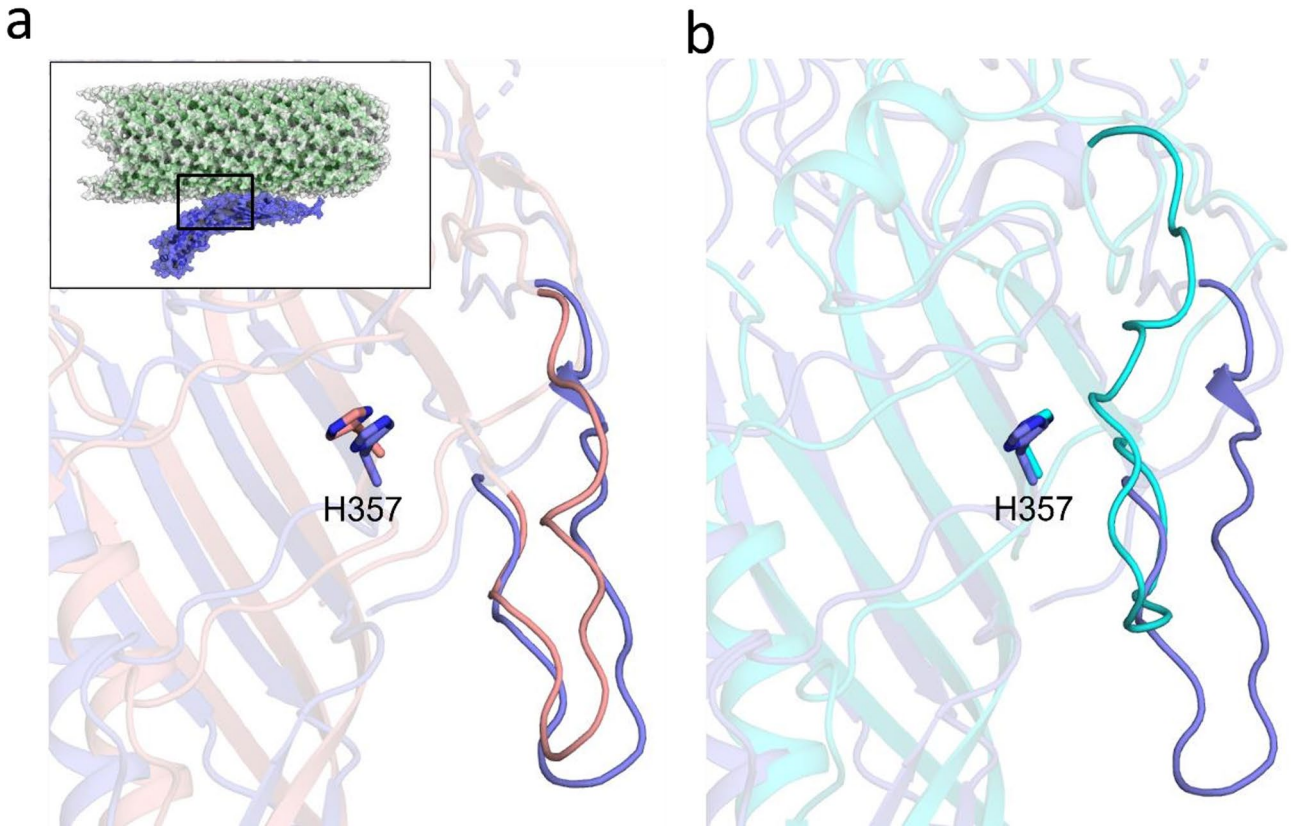



**Fig. 4**. Conformational states of the MP highlighting key loop movements and H357 interactions. (**a**) The inset in the top left corner shows the cryo-EM structure of the MP (PDB ID: 6NM5, shown in purple) interacting with the F-pilus. The rest of panel (**a**) illustrates the cryo-EM experimental structure of the MP (purple cartoon) superimposed onto the "open" loop conformational state (orange cartoon), where the loop (residues L40–P50) enables H357 (shown in sticks) to interact with the F-pilus. (**b**) The cryo-EM experimental structure (purple cartoon) is superimposed onto the "semi-closed" loop conformational state (cyan cartoon), where the loop is in close proximity to H357, restricting its accessibility and preventing direct interaction with the F-pilus. These conformational states demonstrate the importance of "side loop" dynamics in facilitating or restricting critical interactions necessary for viral infectivity

pentameric and hexameric pores. Additionally, ion binding patterns suggest a structural role in maintaining capsid integrity and potentially aiding infectivity under different environmental conditions.

While our simulations provide detailed atomistic insights, they are inherently limited by force field approximations and the absence of viral RNA or host interactions, which warrant experimental validation. Moreover, while our analyses indicate convergence of various local and global viral capsid metrics, we acknowledge that the 0.5 μs trajectories provide limited sampling compared to the longer timescales associated with biological processes such as virus-pilus receptor binding or genome release. Future studies and methods, such as cryo-electron microscopy or NMR spectroscopy could validate our findings and provide deeper insights into the molecular mechanisms driving the observed dynamics. Mutational analyses targeting key residues, particularly those in the loop surrounding H357, may further elucidate the relationship between the MP's structure, dynamics, and function. Such research may guide future rational strategies aimed at disrupting host-virus interactions.

## Methods

### System setup

We used the experimental cryo-EM structure of MS2 (PDB: 5TC1[10] which corresponds to 178 capsid monomers and one MP ($MS2_{MP}$). Since the structure of MP has multiple missing residues (16–34, 71–93, 243–251, 334–345), we used coordinates of MP corresponding to PDB: 6NM5 of the F-pilus/MP complex and structurally aligned it onto the pilus unbound MS2 structure (PDB: 5TC1). The complete MS2 structure without MP ($MS2_{No-MP}$) was taken from PDB: 2MS2[1] and corresponded to 180 monomers of CP alone. In both systems, protein ionizable residue charges were assigned according to neutral pH with charged termini, treated using the CHARMM36m[11] force field. Both systems were subject to energy minimization in vacuum using the steepest descent (SD) algorithm with a 0.01 nm step size and 1,000 kJ $mol^{-1}$ $nm^{-1}$ force tolerance. Each construct was placed in a dodecahedron box with ~32 nm box edge. Approximately 600,000 TIP3P water[12] molecules were uniformly added to the box along with 150 mM NaCl salt ensuring system neutrality and proper ionic concentration.

For the $MS2_{MP}$ system, 191 $Cl^-$ ions were required to neutralize the system, followed by the addition of 2044 $Na^+$ and 2044 $Cl^-$ ions to achieve the 150mM NaCl final concentration. Similarly, for the $MS2_{No-MP}$ system, 180 $Cl^-$ ions were used for neutralization, with an addition of 1903 $Na^+$ and 1903 $Cl^-$ ions added to reach the 150mM concentration. Energy minimization was then performed again using the SD algorithm with the same settings. Each system was equilibrated in three steps with position restraints on protein backbone atoms and a force constant of 1000 kJ $mol^{-1}$ $nm^{-2}$ using: (i) the NVT ensemble for 0.5 ns with a 1 fs time step; (ii) the NPT ensemble for 0.5 ns with a 1 fs time step; and (iii) the NPT ensemble for 5 ns with a 2 fs time step. Both systems were subject to a production run of 500 ns with a 2 fs time step in the NPT ensemble without any restraints.

All simulations were performed using the GROMACS 2018.3 simulation package[13]. A temperature of 300 K was maintained using the velocity rescaling thermostat with an additional stochastic term using a time constant of 1 ps. The pressure was maintained isotropically at 1 atm using the Berendsen barostat[14] during equilibration and the Parrinello-Rahman barostat[15] during the production run and a time constant of 5 ps was used. All bonds which involved hydrogens were constrained using the LINCS algorithm[16]. Equations of motion were integrated using the leap-frog algorithm. Long-range electrostatic interactions were described using the particle mesh Ewald (PME) method[17]. The cut-off distance was 1.2 nm for the short-range neighbour list and van der Waals interactions with a smooth switching function from 1.0 nm. Periodic boundary conditions were applied in all directions. Each simulation was performed on the National Supercomputing Center (https://www.nscc.sg) using 24 nodes with 24 CPUs each (Intel® Xeon® CPU E5-2960 v3 @ 2.60 GHz).

## Analysis

To assess the structural stability of the $MS2_{MP}$ and $MS2_{No-MP}$ systems over the simulation time relative to the initial conformation, root mean square deviation (RMSD) and Principal Component Analysis (PCA) were calculated for protein backbone atoms. The first (PCA1) and second (PCA2) principal components corresponded to 33.2% and 29.4% of the total variance, respectively. Per-residue protein surface occupancy by ions was calculated as a mean over $MS2_{MP}$ and $MS2_{No-MP}$ systems and averaged over all trimers. The occupancy corresponded to the percentage of the total simulation time in which ions and protein residues were within 0.4 nm cutoff distance of one another.

The radius of the pentameric and hexameric pores in the MS2 capsid were determined using the MDAnalysis library[18] in combination with custom Python scripts. For each CP forming the pentameric and hexameric icosahedral complexes, five key residues surrounding the pore were identified and selected for analysis. The residues identified for the pentameric pore were:

D136, K137, E107, T108, H32, and G33, and for the hexameric pore were G121, V123, I126, L129, and I118. The average distances between the centers of mass of these residues were calculated over the last 100 ns of the trajectory. Statistical analysis assessing normality of the data was performed using Shapiro-Wilk test. For the data that followed normal distribution, a parametric t-test with a significance threshold (alpha) set at 0.05 was performed to estimate significance of the observed differences in pore radii between the $MS2_{MP}$ and $MS2_{No-MP}$ systems.

To determine the impact of the MP on the stability of the MS2 capsid, the distribution of salt bridges formed between CPs was analysed. Salt bridges were defined as interactions between the nitrogen atoms of basic residues (lysine and arginine) and the oxygen atoms of acidic residues (glutamate and aspartate) with a distance less than a specified cutoff. MDAnalysis was used to calculate salt bridges between sidechains of basic and acidic residues using a 0.4 nm cutoff distance.

## Data availability

The data supporting this article have been included as part of the Supporting Information. The simulation outputs, analysis scripts and data are available from the corresponding authors upon reasonable request.

Received: 2 June 2025; Accepted: 5 September 2025
Published online: 08 October 2025

## References

1. Golmohammadi, R., Valegård, K., Fridborg, K. & Liljas, L. The refined structure of bacteriophage MS2 at 2.8 Å resolution. *J. Mol. Biol.* **234** (3), 620–639 (1993).
2. Valegård, K., Liljas, L., Fridborg, K. & Unge, T. The Three-Dimensional structure of the bacterial virus MS2. *Nature* **345** (6270), 36–41 (1990).
3. Meng, R., Karslake, J., Manoharan, V. N., Ha, T. & Shakhnovich, E. I. Structural basis for the adsorption of a Single-Stranded RNA bacteriophage. *Nat. Commun.* **10** (1), 3130 (2019).
4. Farafonov, V. S. & Nerukh, D. MS2 bacteriophage capsid studied using All-Atom molecular dynamics. *J. Mol. Biol.* **426** (4), 873–887 (2020).
5. Dent, K. C. et al. The asymmetric structure of an icosahedral virus bound to its receptor suggests a mechanism for genome release. *Structure* **21** (7), 1225–1234 (2013).
6. Spankie, T. J., Haywood, A. L., Dottorini, T., Barrow, P. A. & Hirst, J. D. Interaction of the maturation protein of the bacteriophage MS2 and the sex Pilus of the *Escherichia coli* F plasmid. *J. Mol. Graph Model.* **101**, 107–116 (2020).
7. Thongchol, J., Lill, Z., Hoover, Z. & Zhang, J. Recent advances in structural studies of Single-Stranded RNA bacteriophages. *Viruses* **15** (10). (2023).
8. Chang, J. Y., Gorzelnik, K. V., Thongchol, J. & Zhang, J. Structural assembly of Q beta virion and its diverse forms of Virus-like particles. *Viruses* **14** (2), 225 (2022).
9. Farafonov, V. S., Stich, M. & Nerukh, D. A. Complete virion simulated: All-Atom model of an MS2 bacteriophage with native genome. *J. Chem. Theory Comput.* **19** (10), 4709–4721 (2023).
10. Dai, X. et al. *Situ* structures of the genome and genome-Delivery apparatus in a Single-Stranded RNA virus. *Nature* **541** (7635), 112–116 (2017).

11. Huang, J. et al. Jr. CHARMM36m: an improved force field for folded and intrinsically disordered proteins. *Nat. Methods*. **14** (1), 71–73 (2016).
12. Jorgensen, W. L., Chandrasekhar, J., Madura, J. D., Impey, R. W. & Klein, M. L. Comparison of simple potential functions for simulating liquid water. *J. Chem. Phys*. **79** (2), 926–935 (1983).
13. Van der Spoel, D. et al. GROMACS: fast, flexible, and free. *J. Comput. Chem*. **26** (16), 1701–1718 (2005).
14. Berendsen, H. J. C., Postma, J. P. M., van Gunsteren, W. F., DiNola, A. & Haak, J. R. Molecular dynamics with coupling to an external bath. *J. Chem. Phys*. **81** (8), 3684–3690 (1984).
15. Parrinello, M. & Rahman, A. Polymorphic transitions in single crystals: A new molecular dynamics method. *J. Appl. Phys*. **52** (12), 7182–7190 (1981).
16. Hess, B. L. I. N. C. S. A linear constraint solver for molecular simulations. *J. Comput. Chem*. **18** (12), 1463–1472 (1997).
17. Essmann, U. et al. A smooth particle mesh Ewald method. *J. Chem. Phys*. **103** (19), 8577–8593 (1995).
18. Michaud-Agrawal, N., Denning, E. J., Woolf, T. B. & Beckstein, O. MDAnalysis: A toolkit for the analysis of molecular dynamics simulations. *J. Comput. Chem*. **32** (10), 2319–2327 (2011).
19. Rowsell, S. et al. Crystal structures of a series of RNA aptamers complexed to the same protein target. *Nat. Struct. Biol*. **5** (11), 970–975 (1998).


## Acknowledgements

The computational work for this article was fully performed using the resources of the National Supercomputing Centre, Singapore (https://www.nscc.sg). This research was supported by the Agency for Science, Technology and Research (A*STAR), Singapore, and by The Procter and Gamble Company (P&G) Research Collaboration Agreement. The authors declare that no Artificial Intelligence tools were used for image or text generation.

## Author contributions

Conceptualization: Peter J. Bond, C. Mark Maupin, Stephen J.Fox, Chandra S. Verma, Jiquan Liu. Methodology: Srdan Masirevic, Jan K. Marzinek, Peter J. Bond, Stephen J. Fox. Software: Srdan Masirevic, Jan K. Marzinek. Validation: Srdan Masirevic, Jan K. Marzinek. Formal analysis: Srdan Masirevic, Jan K. Marzinek. Investigation: Srdan Masirevic, Jan K. Marzinek. Resources: Peter J. Bond, C. Mark Maupin, Stephen J. Fox, Chandra S. Verma, Jiquan Liu. Data curation: Srdan Masirevic, Jan K. Marzinek. Writing - Original draft: Srdan Masirevic, Jan K. Marzinek. Writing - Review & Editing: Srdan Masirevic, Jan K. Marzinek, Peter J. Bond. Visualization: Srdan Masirevic, Jan K. Marzinek. Supervision: Peter J. Bond, C. Mark Maupin, Stephen J. Fox, Chandra S. Verma, Jiquan Liu. Project Administration: Peter J. Bond, C. Mark Maupin, Stephen J. Fox, Chandra S. Verma, Jiquan Liu. Funding Acquisition: Peter J. Bond, C. Mark Maupin, Stephen J. Fox.

## Funding

This work was supported by the A*STAR–P&G Joint Collaboration on Hygiene Accelerator Grant of the Agency for Science, Technology and Research (A*STAR), Singapore, and by The Procter and Gamble Company (P&G) [Grant ID: C22HA16012]. We also acknowledge BII (A*STAR) core funds.

## Declarations

## Competing interests

The authors declare no competing interests.

## Additional information

**Supplementary Information** The online version contains supplementary material available at https://doi.org/10.1038/s41598-025-19036-0.

**Correspondence** and requests for materials should be addressed to C.S.V. or P.J.B.

**Reprints and permissions information** is available at www.nature.com/reprints.

**Publisher's note** Springer Nature remains neutral with regard to jurisdictional claims in published maps and institutional affiliations.

**Open Access** This article is licensed under a Creative Commons Attribution-NonCommercial-NoDerivatives 4.0 International License, which permits any non-commercial use, sharing, distribution and reproduction in any medium or format, as long as you give appropriate credit to the original author(s) and the source, provide a link to the Creative Commons licence, and indicate if you modified the licensed material. You do not have permission under this licence to share adapted material derived from this article or parts of it. The images or other third party material in this article are included in the article's Creative Commons licence, unless indicated otherwise in a credit line to the material. If material is not included in the article's Creative Commons licence and your intended use is not permitted by statutory regulation or exceeds the permitted use, you will need to obtain permission directly from the copyright holder. To view a copy of this licence, visit http://creativecommons.org/licenses/by-nc-nd/4.0/.

© The Author(s) 2025